Lab on a Chip

Accepted Manuscript

ROYAL SOCIETY OF CHEMISTRY

www.rsc.org/loc

Cite this: DOI: 10.1039/c0xx00000x

www.rsc.org/xxxxxx

ARTICLE TYPE

Haemoglobin Content Modulated Deformation Dynamics of Red Blood Cells on a Compact Disc

Shantimoy Kar[1], Uddipta Ghosh[2], Tapas Kumar Maiti*[1, 3] and Suman Chakraborty*[1, 2]

Received (in XXX, XXX) Xth XXXXXXXXX 20XX, Accepted Xth XXXXXXXXX 20XX

DOI: 10.1039/b000000x

We investigate the deformation characteristics of red blood cells (RBCs) on a rotating compact disk platform. Our study brings out the interplay between haemoglobin content and RBC's deformability in a centrifugally actuated microfluidic environment. We reveal that RBC's deformations follow the similar trend of principal stress distributed throughout the radial direction, rendering an insight into the mechano-physical processes involved. This study can be used as a diagnostic marker to determine haematological disorders in diseased blood samples tested on compact disk based microfluidic platforms.

Introduction

Haemoglobin (Hb) is the one of the most important constituents of red blood cells (RBCs). Fluctuation in haemoglobin content leads to the occurrence of several physiological disorders. On the other hand, the morphology of RBCs is used as a pertinent marker to diagnose the diseases like malaria[1], anemia, and sickle cell diseases. The deformability of cells (especially deformation of RBC) is crucial to maintain the oxygen level within the tissues, as they deform themselves by keeping the total volume constant[2,3]. The spectrin network which is just beneath the RBC membrane surface is one of the main factors determining the deformability of the cells[4]. Apart from this, haemoglobin is an internal constituent of the RBCs; which affects the internal fluidity of the cells[2]. Deviations of haemoglobin values from a prescribed range are also indicators of physiological abnormalities. In addition, RBC's morphology is greatly dictated by the viscosity of the internal fluid. Alteration in RBC morphology can be achieved by tailoring the haemoglobin (Hb) percentage in the internal fluid. Diagnosis through exploiting cellular rheology has previously been employed in a number of methods, including micropipette aspiration[5], optical tweezers[6], SiMCA[7], di-electrophoresis[8]. Throughout the last two decades, researchers have executed ample investigations to establish a generalized, yet simplified tool for diagnosing haematological disorders. Towards that, studies have been reported in the literature on the deformability of RBCs due to parasitic invasion and also due to the alteration within cytoskeleton network of the membrane[9]. However, the approach of studying cellular deformations with the interplay of Hb is yet to be explored.

In the literature, the combined interplay of fluidic channel geometry and cell morphology[10] is extensively used to diagnose parasitic invasions. In this context, researchers have introduced branched channel geometries for isolating the malaria-infected cells by exploiting the membrane stiffness[11]. Such geometrical features, in effect, create a distribution of forces within the conduit. Distribution of forces throughout the micro-conduits however, can alternatively be achieved through rotational actuation mechanism as well. In addition to the simplicity in altering the pumping characteristics by altering the rotational speeds, the rotationally actuated microfluidic platforms are characterized by some other notable advantages like high sensitivity, negligible dead volume, low chip volume, portable, simpler instrumentations etc. Lab-on-a-compact-disk[12] (LOCD) platform is profoundly efficient for *in-vitro*[13] studies encompassing primary fluidic operations like mixing, metering, decanting, sequential valving, separation [13,14], to name a few[10]. The potent of performing several individual fluidic operations on a single platform makes it more apt for tedious biological experiments like enzyme linked immunosorbent assay (ELISA)[15]. Moreover, the LOCD devices[16,17] have the potential to serve a cost-effective high throughput screening (HTS) platform. With an aim of understanding the haematological disorders in simple and inexpensive way, we have recently shown the effect of hematocrit on blood dynamics in a centrifugally-actuated LOCD platform[18].

In this investigation, we study the deformation dynamics of RBCs on LOCD platform, with the interplay of haemoglobin content. The deformability of the RBCs can be tailored through tuning the internal viscosity of the cells, as dictated by the haemoglobin content. To validate our experimental findings, we have numerically simulated underlying flow process on a rotating platform, considering a suitable constitutive model on blood rheology[19]. From our findings, it is seen that the experimental results show the similar trend as predicted from simulations, thereby providing deep physical insight on the relation between the deformation dynamics of RBCs and the incipient stresses originating from rotational actuation. We envisage that the deformability indices obtained for RBCs at various radial locations on the compact disk platform may be potentially utilised as effective diagnostic markers, as a parametric function of the haemoglobin content.

Materials and Methods

The lab-on-a-CD (LOCD) platforms were fabricated through lamination technique[12,18]. Amongst its five layers, three layers were made of poly-methyl-methacrylate (PMMA) (Lexan, GE) sheets and other two of pressure sensitive double sided adhesives (PSA) (FLEX mount DFM 200 clear V-95, 3M, Flexcon, Inc., Spencer, MA). The microchannels were on the PSA layer, while the reservoirs remained on the middle PMMA layer. All the necessary five layers were attached together to prepare the disk. Fabrication of the channels was executed using a table-top CNC machine (T-Tech Inc. QC 5000). The fabricated LOCD platforms were coupled with a servo motor (SureServo™ AC Servo Systems) for controlled rotations.

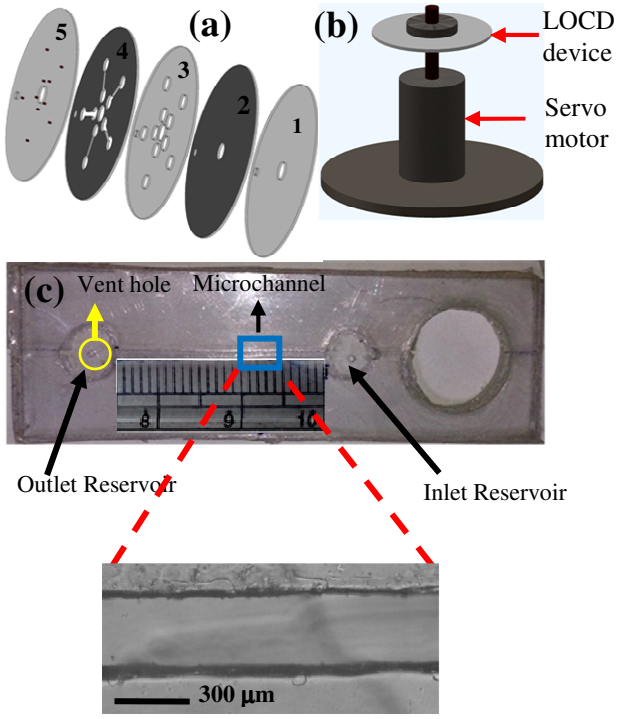

Figure 1:(a) Fabrication of LOCD device. All the five layers are aligned through an alignment hole and are thereafter compressed to obtain the final LOCD device. Amongst five layers, layer 1, 3, 5 consist of PMMA sheets while other two layers are made of pressure sensitive double sided adhesives; **(b)** Depicts a 3D schematic of servo-motor coupled LOCD device;**(c)** shows a single unit(a straight channel attached with inlet and outlet reservoirs) used for the experiments. The microchannel is shown as a blown-up figure.

The LOCD platforms consisted of one single straight micochannel connected between two reservoirs. Dimensions of the fabricated channels were: L=2.4 cm; W= 300 µm; and H= 100 µm, whereas the two reservoirs were of 0.7 cm diameter. The inlet reservoir was designed at 1.5 cm away from the centre. While performing the experiments we kept the samples in the inlet reservoir which is close to the centre. Bottom surface of the devices was functionalized with (3-Aminopropyl)triethoxysilane (APTES) (Sigma Aldrich) and concanavalin-A (Con-A) (Sigma Aldrich) respectively by following the protocols as reported in literature[20]. This particular modification of PMMA surface ensures attachment of RBCs on the surface[21]. 60 µl of diluted blood sample (30 times diluted with 1X phosphate buffer saline (PBS) solution of pH~7.4 (in which [PO_4^{3-}] ~ 10 mM, [NaCl] ~ 137 mM); which does not lead to any kind of deformation for RBCs i.e. this particular concentration of PBS does not alter the osmotic state of RBC[22,23]) has been injected into the inlet reservoir. Initially, we have rotated the LOCD device at a rotational speed of 560 rpm (which is the burst frequency of the device) for 10 seconds, so that the fluid has been transported through the channel and reach till the outlet reservoir. Rotation at 560 rpm for 10 seconds ensures that the blood sample were transported through the entire channel and thereafter incubated for 30 minutes before executing the experiments, which ensures the attachment of RBCs within the channel surface. It is known that the RBCs undergo two different phases of deformations while stresses are being exerted[24]. At initial stage, the cells tend to deform in the direction of the flow and thereafter come back to their initial configuration, if the exerted stress is removed (known as recovery phase). However, if the stresses on the cell exceed a certain value, they undergo a permanent deformation, known as plastic deformation. This is observed after the end of recovery phase. During the experiments, we have rotated the platform for 40 seconds so that the exerted stress on the surface-adhered cells leads to the plastic deformations (in Figure S1 of Electronic Supplementary Information (ESI), we have seen that the plastic deformation stage has been observed at ~ 10s).

All the experiments were conducted following the Institutional ethical guidelines of the authors. Institutional ethical committee approved the experiments (Approval No. IIT/SRIC/AR/2012) and informed consents were taken while collecting the samples from the volunteers. We have chosen blood samples having wide range of haemoglobin (from 7 g/dl to 14 g/dl). The haemoglobin content was measured through using an automated cell counter (Transasia/ Erba Diagnostics (Sysmex KX-21), through which the blood cells were lysed followed by the detection of haemoglobin content through colorimetric approach[25]. By this particular approach, RBCs were first hemolysed and afterwards the released haemoglobin is converted to SLS haemoglobin. The converted SLS haemoglobins are measured by spectrophotometric methods. Hydrophilic groups of SLS bind to the haeme group of haemoglobin and form a stable, coloured complex (SLS-HGB), which is determined following a spectrophotometric method. It is important to note that this particular approach of Hb detection follows a population-based assay, i.e., it represents the average value of Hb for total number of RBCs present in the blood sample. The Hb content in an individual RBC is represented by MCH (haemoglobin amount per red blood cell) index. According to the definition of MCH[26], it varies linearly with the total Hb content of the blood; for that reason we use Hb content of total blood during our study instead of haemoglobin content of a single RBC. Another important point to note here is that, the Hb content of blood, as represented in the present work, in terms of an average value, is the most popularly used pathological indicator of haemoglobin levels in the blood. Therefore, we infer that use of the parameter Hb is well justified for the present study.

During the experimentations, 60 µl of blood sample were injected in the inlet reservoir and thereafter actuated through rotation of servo-motor. After actuating the blood samples under a specific rotational speed, we have captured the images at different radial locations through an inverted microscope (OLYMPUS IX71). During analysis, captured images were post processed using MATLAB. Geometrically, the cells were mapped to ellipses, through edge detection technique. Finally, the deformability indices (DI) were calculated, defined as the ratio of major and minor axes of the ellipse[7]. To differentiate the effect of applied centrifugal field on DI value, we have performed the imaging both before and after the rotational actuation. RBCs have a typical diameter of 6-8 µm and a typical depth of 2 µm, whereas the height of the channel is 100 µm, which is dictated by the thickness of the PSA layers. Therefore the attached RBCs (i.e. the fixed RBCs with the bottom surface) are ~ 100 µm apart from the channel's top wall. Thus the effect of top wall on RBC deformation can be neglected.

Further, to rule out the effect of channel sidewalls we have calculated the DI values of RBCs located within the central zone (within a range of 20 µm from the channel centerline) of the channel. Thus, altogether the influence of the surface properties of the channel walls (apart from the one, to which the cells were attached) was inconsequential for the calculation of RBC deformation.

Numerical Modeling

Since the cell deformation is directly related to the exerted stress on it, the stress distribution can give us a qualitative estimate of the cell deformation throughout the radial extent. To investigate the stress distribution along the radial direction, we have performed numerical simulations using COMSOL Multiphysics 4.2, considering a channel of height H and length L, connected between two reservoirs at the two ends. The origin is placed on the bottom wall, with the x axis running in the axial direction and the y axis running vertically (as shown in figure 2). To actuate the fluid flow along the channel, the channel is subjected to a rotation around the centerline. We consider our frame of reference to be rotating with respect to the channel. Considering the burst frequency of the platform to be 560 ± 20 rpm as obtained experimentally, we have executed our simulations for three different frequencies: 560 rpm, 750 rpm and 2050 rpm. Further,

for computational implementation, we consider $W \gg H$, so that the flow can be assumed to be two dimensional, which significantly reduces the required computational expenses and mimics our experimental scenario where we investigate the effect of exerted stress on RBCs, which are adhered on the bottom surface of the channel. In an effort to justify the use of 2D simulations, we have performed a comparative study between the results of 2D and 3D simulations, for a simple geometry. For the sake of brevity, the results have been presented in the supporting material (Figure S2 of ESI) with this study. These results clearly depict that 2D simulations predict the stress distribution very accurately, even for a W/H ratio of 3.

While executing the simulations, we have considered the constitutive behavior of blood defined through blood-morphology dependent power-law model[19,27].

With the aforementioned assumptions, the equation of motion for the fluid in the channel can be written in the following form (steady flow):

$$\rho \mathbf{v}\cdot\nabla\mathbf{v} = -\nabla p + \nabla\cdot\boldsymbol{\tau} + \left(\rho\omega^2 x\right)\mathbf{e_x} \qquad (1.a)$$

$$\nabla\cdot\mathbf{v} = 0 \qquad (1.b)$$

Here, $\boldsymbol{\tau}$ is the stress tensor, ω is the rotation speed of the platform and $\mathbf{e_x}$ is the unit vector along the x direction, while other symbols bear their usual meanings. For power law model, the stress-strain relation is given by:

$$\tau_{ij} = 2m\left|\gamma\right|^{n-1}\gamma_{ij} \quad (2.a)$$

$$\text{where, } \dot{\gamma}_{ij} = \frac{1}{2}\left(\frac{\partial u_i}{\partial x_j} + \frac{\partial u_j}{\partial x_i}\right) \quad (2.b)$$

In equation (2.a – 2.b), m is consistency index and n is the behavioral index. The quantity $\left|\gamma\right|$ is defined as follows:

$$\left|\gamma\right| = \sqrt{\frac{1}{2}\gamma:\gamma} = \sqrt{\frac{1}{2}\gamma_{ij}\gamma_{ij}} \quad (2.c)$$

A number of previous studies[19] have derived empirical relations between the hematocrit fraction of the blood and the corresponding values of n and m in the constitutive relation (2.a). The mathematical expressions relating n and m to hematocrit fraction and TPMA (total protein minus albumin) content in the blood are as follows[27]: $n = 1 - hC_3$; $m = 0.1C_1 e^{C_2 h + \frac{C_4 T}{h^2}}$ (3)

In (3), h is the hematocrit fraction and T is the TPMA content in the blood. C_1, C_2, C_3 and C_4 are constants, whose values are taken as follows[27]: C_1 = 0.0797, C_2 = 0.0608, C_3 = 0.00499 and C_4 = 14.585. As an example, we note that for h = 0.38 and T = 25.9, we get, n = 0.81 and m = 0.104.

We non-dimensionalize the equations (1) with the following scheme: $\bar{x},\bar{y} = x/H, y/H; \bar{u},\bar{v} = u/u_0, v/u_0$; $\bar{p} = p/\tau_{ref}H$ and $\bar{\tau} = \tau/\tau_{ref}, \tau_{ref} = m\left(u_0/H\right)^n$. We accordingly define $\gamma_{ref} = u_0/H$ and

$$\left|\bar{\gamma}\right| = \left[\frac{1}{2}\left(\frac{\partial\bar{u}}{\partial\bar{x}}\right)^2 + \frac{1}{2}\left(\frac{\partial\bar{v}}{\partial\bar{y}}\right)^2 + \frac{1}{4}\left(\frac{\partial\bar{u}}{\partial\bar{y}} + \frac{\partial\bar{v}}{\partial\bar{x}}\right)^2\right]^{1/2}.$$ The reference velocity is taken as: $u_0 = \left(\rho\omega_0^2 H^{n+2}/m\right)^{1/n}$, where ω_0 is the burst frequency. The non-dimensional equation in a vector form is finally expressed as:

$$\mathrm{Re}^*\left(\bar{\mathbf{v}}\cdot\bar{\nabla}\bar{\mathbf{v}}\right) = -\bar{\nabla}\bar{p} + \bar{\nabla}\cdot\bar{\boldsymbol{\tau}} + \left(R^2\bar{x}\right)\mathbf{e_x}; \bar{\nabla}\cdot\bar{\mathbf{v}} = 0 \qquad (4)$$

In equation (3), $R^2 = \omega^2/\omega_0^2$ and $\mathrm{Re}^* = \rho u_0^{2-n}H^n/m$ is the modified Reynolds number. To evaluate the stress distribution, we seek to obtain the principle stress in the channel, estimated from the shear and normal components of stresses as calculated

from the solution to equation (4) with the help of equations (2.a – 2.b). The principal stresses[28] are given by:

$$\bar{\sigma}_1 = \frac{\bar{\tau}_{xx} + \bar{\tau}_{yy}}{2} + \sqrt{\left(\frac{\bar{\tau}_{xx} - \bar{\tau}_{yy}}{2}\right)^2 + \bar{\tau}_{xy}^2} \quad (5.a)$$

$$\bar{\sigma}_2 = \frac{\bar{\tau}_{xx} + \bar{\tau}_{yy}}{2} - \sqrt{\left(\frac{\bar{\tau}_{xx} - \bar{\tau}_{yy}}{2}\right)^2 + \bar{\tau}_{xy}^2} \quad (5.b)$$

$$\bar{\tau} = \sqrt{\left(\frac{\bar{\tau}_{xx} - \bar{\tau}_{yy}}{2}\right)^2 + \bar{\tau}_{xy}^2} \quad (5.c)$$

Here, σ_1, σ_2 are the principal normal stresses and τ is the principal shear stress. We have used no-slip boundary condition at the walls and zero gauge pressure has been assumed at the open ends.

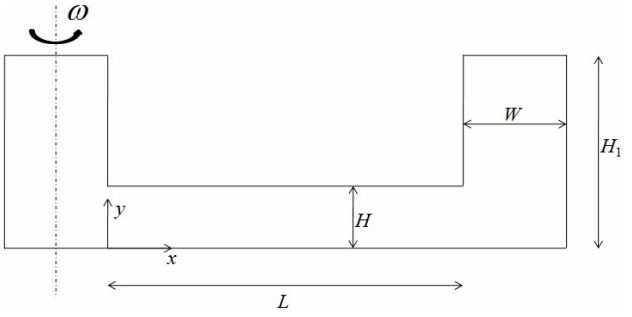

Figure 2: Schematic of the geometry used for numerical simulation. The channel consists of two reservoirs of height H_1, width W, while the channel is of height H and length L. The channel width has been assumed to be much larger than the channel height. The whole channel rotates around axis shown by the dotted line. The angular speed of rotation has been denoted as ω.

Results and Discussions

It is a well known fact that centrifugal and Coriolis forces work over a rotating disk platform[29]. These two forces lead to the deformations of RBCs attached within the channel surface. Fixation of RBCs on the bottom surface of the channel restricts the flipping and tumbling motions of RBCs. Deformations of RBCs are characterized through deformability index (DI) defined as the ratio of major and minor axes while we map RBCs with an ellipse. It is known that the RBCs get deformed when they are subjected to external stresses and attempt to initialize once the stress is relaxed. Elastic and viscous properties of the cells are the two determining factors of its membrane deformability. Apart from these two key factors, there are few additional issues which also take care of the deformation of RBCs: (1) The cytoplasmic viscosity which is mainly guided by the extent of haemoglobin present there and (2) the biconcave discoid shape enables it to make change of its shape keeping the overall volume constant. For that reason, we investigate the effect of haemoglobin content of blood samples in RBC's deformation. When the haemoglobin percentage is less than standard value, it is expected that the cytoplasmic viscosity of the internal fluid of the RBC will be reduced. As a direct consequence of that, we can expect more deformability from the RBCs while actuated under same rotational speed.

In figure 3, we have shown the deformation characteristics of RBCs at 16 mm away from the centre, for different rotational speeds for RBCs differing in their haemoglobin content. Figure 3 has two important aspects which have been explained separately. Firstly, it is worth noting here that at a rotational speed of 560 rpm, DI values for RBCs having different haemoglobin content shows insignificant variation. This particular observation can be explained by the fact that a speed of 560 rpm is the lowest possible rotational speed (i.e. the burst frequency) for our system. Hence, the exerted stress for 560 rpm is not sufficient to make permanent deformation of RBCs. Thus for a wide range of haemoglobin contents the DI values are almost constant. Considering an ideal biconcave shape of RBC, it can be stated that DI value should be one when there is no deformation. In case of 560 rpm, observed DI values lies within a range of 1.08-1.12 (i.e. little higher than 1), is attributable to the fact of surface adherence of the RBCs on the functionalized PMMA surface. It is an interesting fact to note that the RBCs having haemoglobin content of 11.2 g/dl exhibit the highest deformability (DI value ~ 1.32 ± 0.55 for 750 rpm and 1.42 ± 0.071 for 2050 rpm). Thereafter, a descending trend of DI is followed with the increase of haemoglobin content. Higher the haemoglobin value, higher is the internal viscosity of RBC; which is manifested through lower value of DI. Given the same applied stress, it is intuitive to expect more deformability of RBC having lower haemoglobin percentage. From figure 3, it can however be stated that the fact is not true for all values of haemoglobins.

Secondly, it is seen that the DI values are very small (~ 1.077± 0.029) for the RBCs having haemoglobin content of 7 g/dl and 9.2 g/dl. This observation can be explained by the fact that blood samples having the haemoglobin in a range of 9 g/dl or less than that are known to be anemic. RBCs having lower haemoglobin content (below 10 g/dl) are morphologically different in comparison to RBCs having standard haemoglobin value (~ 11-14 g/dl) (shown in figure S3 of the ESI). Thus, it can be inferred that for anemic blood samples, RBCs undergo insignificant deformation (DI value is < 1.1).

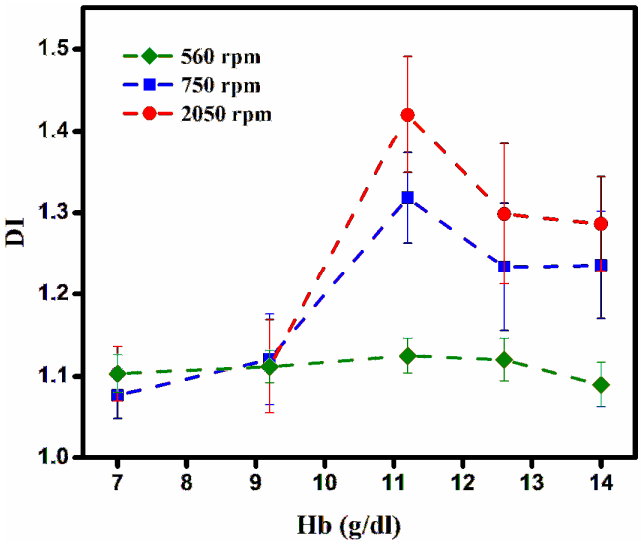

Figure 3: Deformation characteristics as a function of haemoglobin content of the blood samples for different rotational speeds. The error bars represent the standard deviations (s.d.) of the results obtained from four repeated sets of experiments.

From figure 3, it is also evident that for a particular value of haemoglobin (for a range of 11.2 g/dl to 14 g/dl),the increase in the rotational speed indeed causes more deformation (as signified by the higher DI values for RPM 2050), which is very obvious as the extent of exerted stress has been increased with the increase of the rotational speed.

Figure 4a represents the deformation characteristics of RBCs along the radial position of the channel. The maximum deformation of RBC is observed somewhere near the middle of the channel, whereas the RBCs at the two ends of the straight channel are seen to undergo very small deformation (as shown in figure 4a). This specific trend of deformation of RBC can be explained by stress distribution along the radial distance of the channel. In figure 4b, the distribution of principal stress (σ_P , normalized by the maximum stress) has been shown along the radial location of the channel. This stress distribution is a combined consequence of induced pressure and the centrifugal forces acting on the fluid. In this regard, the difference in characteristics for a dilute aqueous solution and a blood sample may be carefully noted. From an order of magnitude sense, considering a dilute aqueous solution, the centrifugal force ($F_w = \rho r\omega^2$) scales as $O\left(10\omega^2\right)$ and the Coriolis force scales as $F_C \sim 2\rho U\omega$. Now, the order of magnitude of velocity can be evaluated by balancing the viscous and the centrifugal forces, which takes the form[12,30]: $U \sim \frac{D_h^2 \rho r\omega^2}{32\eta_{eff}}$, where D_h is the hydraulic diameter of the channel, η_{eff} is the effective viscosity of the sample, and rest of the symbols bear usual meaning as defined before. Using the values of the geometric parameters of the present study and a dilute aqueous solution, we note that this velocity is approximately of O ~ $10^{-5}\omega^2$ m/s and therefore, the Coriolis force is of the order of ~ $O(0.01\omega^3)$. Thus the ratio of centrifugal to Coriolis force $\beta = F_w / F_c$, scales as $O\left(1000\omega^{-1}\right)$, for a dilute aqueous solution. However, in the present investigation blood is considered to be the fluid medium, which has an effective viscosity in the range of[18,31] ~ 5.3 cP at low shear rate ~ 10 s^{-1}, for hematocrit level 0.37. Therefore, for blood the velocity U is the tune of ~ $10^{-6}\omega^2$ m/s, which makes $F_c \sim O(0.001\omega^3)$. Thus, the value of β comes out to be ~50 for a rotational speed of 2050 rpm. Therefore, it can be easily inferred that the effect of centrifugal force dominates over the acting Coriolis force (at least larger by an order), in our experiments. In our study, the centrifugal and Coriolis force will be comparable for blood, if the rotational speed can be elevated to 9000 rpm or more, which is significantly beyond the range of speeds investigated in our work. Not only that, such high rotational speeds lead to significant vibrations of the experimental setup, which may alter the accuracy of experimental readouts to an appreciable extent. For that reason, the effect of Coriolis force is not investigated in our study.

We further note that, figure 4b represents only a qualitative variation in the stress distribution along the channel and predicts the overall trend of the stresses acting on the cell. Therefore, from this figure one can infer, how a cell is expected to deform as it is positioned at various locations along the channel. Considering the interplay of forces delineated as above, it intuitively follows from figure 4b that the cells would witness the maximum amount of stress when they are near the middle of the channel and hence the corresponding deformations will also be highest at that point. This conclusion is corroborated from the experimental findings as shown in figure 4a and the theoretical findings in figure 4b. An important point to note from the present figure is that the stresses come out to be positive, which indicates that these are tensile in nature and the cells ought to be stretched by them. Indeed, the experimental results depict that the cells tend to get stretched in due course of flow, as indicated by the deformation index (DI).

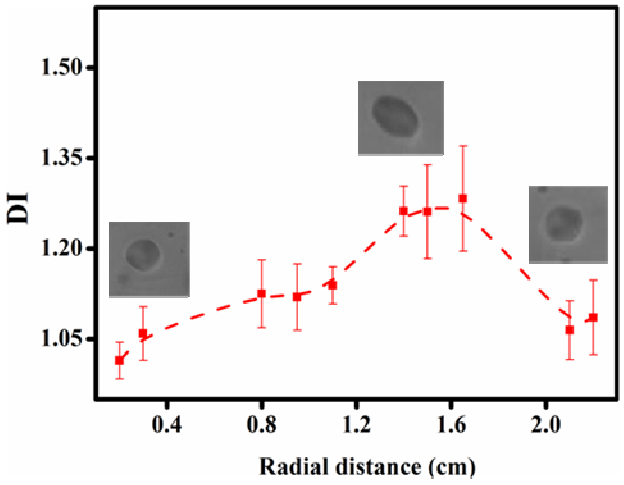

Figure 4a: Characteristic variations of deformability index (DI) along the radial direction of the channel. The deformation of RBCs is evident to be maximum at the middle of the channel. The error bars represent th standard deviations (s.d.) of the results obtained from four repeated sets of experiments.

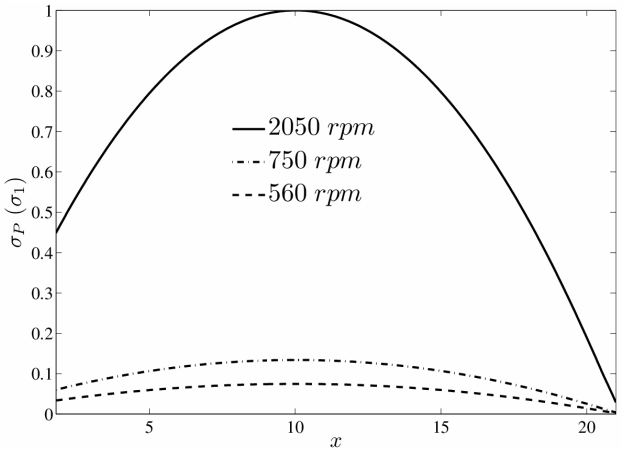

Figure 4b: The simulation results show principal stress (σ_P) distribution along the channel. The simulations were performed for a hematocrit value of *h*= 0.38 (which roughly mimics the experimental condition of haemoglobin content of 12.8; as hematocrit value roughly 3 times of the

haemoglobin content. Normalized principal stress has been plotted in against normalized distance along the radial direction.

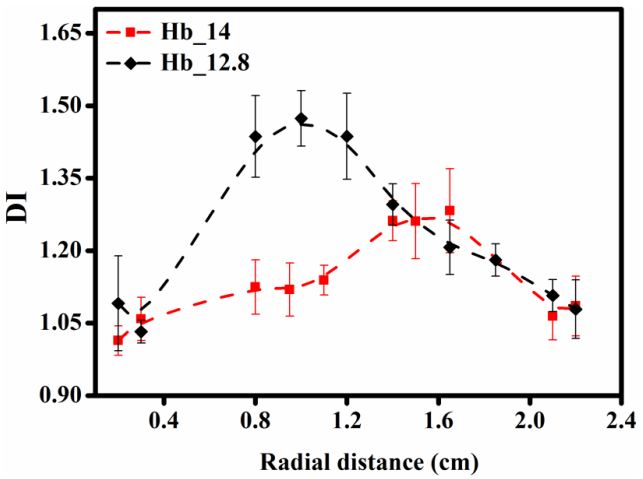

Figure 5: A comparative plot of deformation characteristics of RBCs having different haemoglobin contents, for a rotational speed of 750 rpm. In case of lower haemoglobin content, the maximum deformation was observed at shorter distance as compared to that of the higher haemoglobin value. The error bars represent the standard deviations (s.d.) of the results obtained from four repeated sets of experiments.

In Figure 5, it is clearly seen that sample having haemoglobin content of 12.8 g/dl shows larger deformation as compared to that with 14g/dl. RBCs residing at the middle of the channel show more deformation (~ 31% at a distance of 1 cm away from the centre) whereas the deformations for the two haemoglobin contents are comparable near the channel ends. From figure 4b, it is evident that σ_p attains its maximum value somewhere at the middle of the channel whereas it is low at both the ends. Therefore, one possible explanation for the relatively larger differences in the DI for the two values of haemoglobin, as evident from figure 5, can be given as follows. We can infer that the high values of σ_p at the centre of the channel causes the cells to undergo more deformation, which ultimately results in a large difference in the DI for two different haemoglobin values. However, as we move towards the two ends of the channel, the lower values of stresses are not able to alter the cellular deformation significantly, which causes smaller difference in the DI values, as notable from figure 5.

Conclusions

In conclusion, we have investigated the RBC deformations with interplay of haemoglobin (for a range of 7 g/dl to 14 g/dl) on rotationally actuated microfluidic platform. Our study unveils the interesting biophysics of RBCs under different stressed conditions. Here we highlight that high content of haemoglobin imparts more degree of rigidity to the cell by increasing the internal viscosity of the cells, which in turn dictates the state of stress under the various forces acting on a rotating platform. In this context, we envision that our findings may potentially be utilized to determine the haemoglobin induced disorders by measuring the deformability index (DI) on a simple rotational platform.

Notes and references

[1]Advanced Technology Development Centre, Indian Institute of Technology Kharagpur, Kharagpur-721302; [2]Department of Mechanical Engineering, Indian Institute of Technology Kharagpur, Kharagpur-721302, India; [3]Department of Biotechnology, Indian Institute of Technology Kharagpur, Kharagpur-721302.
Email: suman@mech.iitkgp.ernet.in.
† Electronic Supplementary Information (ESI) available: See DOI: 10.1039/b000000x/

Acknowledgement: This problem has been investigated under the project entiled 'Lab on-a-CD Platform for Malaria Diagnosis'.S.K would like to thank Council of Scientific and Industrial Research (CSIR), India for his research fellowship.

References:

1 L. H. Miller, D. I. Baruch, K. Marsh and O. K. Doumbo, *Nature*, 2002, **415**, 673.
2 O. K. Baskurt and H. J. Meiselman, *Semin. Thromb. Hemost.*, 2003, **29**, 435–450.
3 M. Diez-Silva, M. Dao, J. Han, C.-T. Lim and S. Suresh, *MRS Bull.*, 2010, **35**, 382–388.
4 N. Mohandas and P. G. Gallagher, *Blood*, 2008, **112**, 3939.
5 G. Bao and S. Suresh, *Nat. Mater.*, 2003, **2**, 715.
6 G. Y. H. Lee and C. T. Lim, *Trends Biotechnol.*, 2007, **25**, 111–8.
7 I. Doh, W. C. Lee, Y.-H. Cho, a P. Pisano and F. a Kuypers, *Appl. Phys. Lett.*, 2012, **100**, 173702–1737023.
8 P. Gascoyne, C. Mahidol, M. Ruchirawat, J. Satayavivad, P. Watcharasit and F. F. Becker, *Lab Chip*, 2002, **2**, 70.
9 M. Diez-Silva, M. Dao, J. Han, C.-T. Lim and S. Suresh, *MRS Bull.*, 2011, **35**, 382–388.
10 H. W. Hou, A. A. S. Bhagat, A. G. L. Chong, P. Mao, K. S. W. Tan, J. Han and C. T. Lim, *Lab Chip*, 2010, 2605.
11 H. W. Hou, A. A. S. Bhagat, A. G. L. Chong, P. Mao, K. S. W. Tan, J. Han and C. T. Lim, *Lab Chip*, 2010, **10**, 2605–13.
12 M. Madou, J. Zoval, G. Jia, H. Kido, J. Kim and N. Kim, *Annu. Rev. Biomed. Eng.*, 2006, **8**, 601–28.
13 R. Gorkin, J. Park, J. Siegrist, M. Amasia, B. S. Lee, J.-M. Park, J. Kim, H. Kim, M. Madou and Y.-K. Cho, *Lab Chip*, 2010, **10**, 1758–73.
14 J. Ducrée, S. Haeberle, S. Lutz, S. Pausch, F. Von Stetten and R. Zengerle, *J. Micromechanics Microengineering*, 2007, **17**, S103–S115.
15 S. Lai, S. Wang, J. Luo, L. J. Lee, S. Yang and M. Madou, *Anal. Chem.*, 2004, **76**, 1832.
16 J. Steigert, M. Grumann, T. Brenner, L. Riegger, J. Harter, R. Zengerle and J. Ducree, *Lab Chip*, 2006, **6**, 1040.
17 S. Haeberle, J. Ducree, S. Lutz, S. Pausch, F. V. Stetten and R. Zengerle, *J. Micromechanics Microengineering*, 2007, **17**, 103–115.
18 S. Kar, M. Dash, T. K. Maiti and S. Chakraborty, *Analyst*, 2015, **140**, 1432–7.
19 R. L. Fournier, *Basic Transport Phenomena in Biomedical Engineering*, CRC Press, The University of Toledo Ohio, USA, 3rd edn.
20 B. Roy, T. Das, T. K. Maiti and S. Chakraborty, *Anal. Chim. Acta*, 2011, **701**, 6–14.

21 D. Guerry, M. A. Kenna, A. D. Schrieber and R. A. Cooper, *J. Exp. Med.*, 1976, **144**, 1695–1700.

22 A. R. Minerick, A. E. Ostafin and H. C. Chang, *Electrophoresis*, 2002, **23**, 2165–2173.

23 S. Kar, T. K. Maiti and S. Chakraborty, *Analyst*, 2015, **140**, 6473–6476.

24 B. Roy, D. Carugo, X. Zhang, T. K. Maiti and S. Chakraborty, in *16th International Conference on Miniaturized Systems for Chemistry and Life Sciences*, Okinawa, Japan, 2012, pp. 1003–1005.

25 K. Fujimoto, *Sysmex J. Int.*, 1999, **9**, 31–44.

26 P. R. Sarma, *Clin. Methods Hist. Phys. Lab. Exam.*, 1990, 720–723.

27 S. Chakraborty, *Lab Chip*, 2005, **5**, 421–430.

28 S. P. Timoshenko, *Strength of Materials*, D. Van Nostrand Company, New York, 1930.

29 D. Chakraborty, R. Gorkin, M. Madou, L. Kulinsky and S. Chakraborty, *J. Appl. Phys.*, 2009, **105**, 084904.

30 J. Ducrée, S. Haeberle, T. Brenner, T. Glatzel and R. Zengerle, *Microfluid. Nanofluidics*, 2005, **2**, 97–105.

31 J. J. Bishop, a S. Popel, M. Intaglietta and P. C. Johnson, *Biorheology*, 2001, **38**, 263–274.